Published in final edited form as:
Neuroimage. 2010 May 1; 50(4): 1690–1701. doi:10.1016/j.neuroimage.2010.01.002.

Inter-Individual Differences in Resting State Functional Connectivity Predict Task-Induced BOLD Activity

Maarten Mennes[1], **Clare Kelly**[1], **Xi-Nian Zuo**[1], **Adriana Di Martino**[1,2], **Bharat Biswal**[1,3,4], **F. Xavier Castellanos**[1,4], and **Michael P. Milham**[1]

[1]Phyllis Green and Randolph Cōwen Institute for Pediatric Neuroscience at the NYU Child Study Center, New York, NY

[2]Division of Child and Adolescent Neuropsychiatry, Department of Neuroscience, University of Cagliari, Italy

[3]Department of Radiology, University of Medicine and Dentistry of New Jersey, Newark, NJ

[4]Nathan Kline Institute for Psychiatric Research, Orangeburg, NY

Abstract

The resting brain exhibits coherent patterns of spontaneous low-frequency BOLD fluctuations. These so-called resting-state functional connectivity (RSFC) networks are posited to reflect intrinsic representations of functional systems commonly implicated in cognitive function. Yet, the direct relationship between RSFC and the BOLD response induced by task performance remains unclear. Here we examine the relationship between a region's pattern of RSFC across participants, and that same region's level of BOLD activation during an Eriksen Flanker task. To achieve this goal we employed a *voxel-matched* regression method, which assessed whether the magnitude of task-induced activity at each brain voxel could be predicted by measures of RSFC strength for the same voxel, across 26 healthy adults. We examined relationships between task-induced activation and RSFC strength for 6 different seed regions (Fox et al., 2005), as well as the "default mode" and "task-positive" resting-state networks in their entirety. Our results indicate that, for a number of brain regions, inter-individual differences in task-induced BOLD activity were predicted by one of two resting-state properties: 1) the region's positive connectivity strength with the task-positive network, or 2) its negative connectivity with the default mode network. Strikingly, most of the regions exhibiting a significant relationship between their RSFC properties and task-induced BOLD activity were located in *transition zones* between the default mode and task-positive networks. These results suggest that a common mechanism governs many brain regions' neural activity during rest and its neural activity during task performance.

Keywords

resting-state; task activity; intrinsic representation; voxel-matched; transition zones

Corresponding Author: Michael P. Milham, Phyllis Green and Randolph Cōwen Institute for Pediatric Neuroscience at the NYU Child Study Center, 215 Lexington Ave. 14th Floor, 10016 New York, NY, USA. Phone: +1 212 263 2748; Fax +1 212 263 4675; michael.milham@nyumc.org.

Introduction

Central to adaptive brain function is the ability to recruit appropriate brain regions for the task at hand. Task-based neuroimaging research has led to substantial advances in our understanding of the regions involved in the performance of a given task. Nevertheless, the extent to which functional systems related to task performance are predefined remains poorly understood. Resting-state functional connectivity (RSFC) studies suggest that the functional systems observed during task performance are intrinsically represented in the brain by coherent low-frequency (< 0.1 Hz) fluctuations in the BOLD signal within distinct functional networks (Biswal et al., 1995; Damoiseaux et al., 2006; Fox and Raichle, 2007; Fox et al., 2005; Greicius et al., 2003; Kiviniemi et al., 2009; Margulies et al., 2007; Vincent et al., 2007). Numerous studies have drawn attention to similarities between patterns of task-based activation and functional networks detected during rest (Greicius and Menon, 2004; Smith et al., 2009; Thomason et al., 2008; Toro et al., 2008). However, no study has directly linked resting state phenomena and task-related BOLD activity in the same group, and little is known about the relevance of intrinsic RSFC for task-related neural activity.

Here we examine the extent to which inter-individual differences in a region's task-induced BOLD response can be predicted by inter-individual differences in that region's RSFC characteristics. To tackle this issue we took advantage of the availability of a dataset that included both resting state and Eriksen Flanker Task scans in the same set of 26 participants (Kelly et al., 2008). The Eriksen Flanker Task is commonly used to probe attention and has well-characterized activation patterns (Brown, 2009; Bunge et al., 2002; Ochsner et al., 2009). As such, we aimed to identify one or more well-characterized, easily reproducible, and highly reliable functional networks that are thought to overlap with patterns of activation or deactivation during performance of attentional paradigms such as the flanker task. Accordingly, we selected two of the most commonly studied large-scale networks in the resting state literature, namely the "task positive" and "default mode" networks (Fox et al., 2005). Specifically, across 26 participants, we relate the magnitude of each voxel's BOLD responses evoked during Eriksen Flanker Task performance to the same voxel's RSFC with the default mode and task-positive networks as previously defined by Fox et al. (2005). Regions within the default mode or "task-negative" network typically show a negative BOLD response (or deactivation) during goal-directed tasks and include areas such as ventromedial prefrontal, posterior cingulate, lateral parietal, medial temporal cortex and precuneus (Dosenbach et al., 2007; Fox et al., 2005; Toro et al., 2008). In contrast, the task-positive network comprises regions that are typically activated during performance of stimulus- and goal-directed cognitive tasks. Areas in this network include the frontal eye fields, mid-cingulate cortex, intraparietal sulcus and inferior parietal cortex (Dosenbach et al., 2007; Fox et al., 2005; Toro et al., 2008). Given the implication of the default mode and task-positive networks in both cognitive performance and the resting-state, these networks provide an ideal starting ground to explore the potential of resting-state fMRI measures for explaining BOLD activity induced by task performance.

Since default mode regions typically deactivate during task performance, we predicted that greater RSFC strength with default mode network regions would be associated with lower task-induced BOLD response magnitudes. In contrast, task-positive regions are typically activated during task performance, warranting the prediction that greater RSFC strength with task-positive network regions would be associated with higher task-induced BOLD response magnitudes. To test our predictions, we used a variant of the general linear model approach typically employed for analyses in functional neuroimaging. In the standard approach, effects of interest across all voxels in the brain are detected using the same model for each voxel. In contrast, we employed a unique linear regression model for each voxel, an approach we refer to as *voxel-matched regression*. Specifically, for each participant, we first calculated RSFC

between each voxel and each of the six seed regions previously used to define the default mode and task-positive networks (Fox et al., 2005). Next, for the same participants, we calculated each voxel's BOLD response during performance of the Eriksen Flanker task. Finally, using a unique linear regression model for each voxel, we assessed the relationship between a voxel's RSFC strength for each of the six seed regions, and the magnitude of that same voxel's task-induced BOLD response across participants. While the present work is exploratory in nature, it is worth noting that areas characterized by greater variability in RSFC strength across participants have a greater likelihood of exhibiting meaningful variation (with respect to RSFC/task relationships), compared to areas that are relatively invariant across participants. In this regard, we draw attention to the boundary areas (i.e., edges) of the RSFC networks. They are sharply defined for any given participant (Cohen et al., 2008), but the specific locations of the boundaries are most likely to vary across participants.

Beyond the individual component regions of the default mode and task-positive networks, we assessed the relationship between a voxel's task-induced BOLD response and its connectivity with each of the two networks in their entirety. This allowed for a more general, integrated assessment of the relationship between task-induced activity and the two resting-state networks in their entirety, as compared to assessing that relationship at the level of singular parts (small seed ROIs) of these networks. We predicted that the patterns of RSFC/task-induced activity relationships would be similar those observed for the individual seed regions within the networks. Finally, to assure that our findings were not related to methodological factors of the seed-based approach for measuring RSFC or driven by the a priori selection of seed ROIs, we performed Independent Component Analysis (ICA) to identify RSFC with a default mode component and similarly used this RSFC measure to predict the BOLD activity induced by the Eriksen Flanker task.

Methods

Participants and Experimental Paradigm

The present work used a dataset previously published by our laboratory (Kelly et al., 2008). Twenty-six right-handed adults (age: 28.1 ± 8.5 years) participated in this event-related fMRI study. Participants provided signed informed consent in accordance with the institutional review boards of NYU and the NYU School of Medicine, and were financially compensated for their participation. Two 5-minute functional scans were administered while participants completed a slow event-related Eriksen Flanker Task (inter-trial interval (ITI) varied between 8 s and 14 s; mean ITI = 12 s). On each trial of this task, participants used one of two buttons on a response pad to indicate the direction of a central arrow in an array of 5 arrows. In congruent trials the flanking arrows pointed in the same direction as the central arrow (e.g., > > > > >), while in more demanding incongruent trials the flanking arrows pointed in the opposite direction (e.g., > > < > >). Each run contained 12 congruent and 12 incongruent trials, presented in a pseudorandom order. In addition, participants completed a brief (6.5 min) resting-state scan during which participants were asked to relax while keeping their eyes open. The resting-state scan was always acquired before the Flanker task scans.

Data Acquisition

Functional imaging data were acquired using a research-dedicated Siemens Allegra 3.0 T scanner, with a standard Siemens head coil, located at the NYU Center for Brain Imaging. During each of the two Flanker Task blocks we obtained 146 contiguous echo planar imaging (EPI) whole-brain functional volumes (TR = 2000 ms; TE = 30 ms; flip angle = 80°, 40 slices, matrix = 64 × 64; FOV = 192 mm; acquisition voxel size = 3 × 3 × 4 mm). Stimuli were back-projected onto a screen at the head of the scanner bore and were viewed by participants via an angled mirror that was affixed to the MRI head coil. The resting-state scan comprised 197

contiguous EPI whole-brain functional volumes (TR = 2000 ms; TE = 25 ms; flip angle = 90°, 39 slices, matrix = 64 × 64; FOV = 192 mm; acquisition voxel size = 3 × 3 × 3 mm). Finally, a high-resolution T1- weighted anatomical image was acquired using a magnetization prepared gradient echo sequence (MPRAGE, TR = 2500 ms; TE = 3.93 ms; TI = 900 ms; flip angle = 8°; 176 slices, FOV = 256 mm).

Image Preprocessing

Both Flanker Task scans and the resting-state scan were preprocessed as follows. AFNI (Cox, 1996) was used to perform the initial preprocessing steps of slice timing correction for interleaved acquisition (using Fourier-space time-series phase-shifting), motion correction (by aligning each volume to the mean image using Fourier interpolation) and despiking (detection and reduction of extreme time series outliers). All other data processing was carried out using FSL (www.fmrib.ox.ac.uk). Further image preprocessing comprised spatial smoothing using a Gaussian kernel of FWHM 6mm and mean-based intensity normalization of all volumes by the same factor. The data were then temporally filtered using both a high-pass (Gaussian-weighted least-squares straight line fitting, with sigma = 100.0s) and low-pass filter (Gaussian low-pass temporal filtering: HWHM 2.8s).

Registration of each participant's high-resolution anatomical image to a common stereotaxic space (the Montreal Neurological Institute 152-brain template (MNI152); $2mm^3$ resolution) was accomplished using a two-step process (Andersson et al., 2007). First, a 12 degrees of freedom linear affine was carried out using FLIRT (Jenkinson et al., 2002; Jenkinson and Smith, 2001). Subsequently, the registration was further refined using FNIRT nonlinear registration (Andersson et al., 2007). The resulting transformation was then applied to each participant's functional dataset.

Movement Parameters

Movement in each of the cardinal directions (X, Y and Z) and rotational movement around 3 axes (pitch, yaw and roll) were calculated for each participant. Data were also visually inspected for movement-related artifacts.

Nuisance Signal Regression

In order to control for the effects of physiological processes such as fluctuations related to motion, and cardiac and respiratory cycles, we removed signal associated with several nuisance covariates from the preprocessed images (Kelly et al., 2009b). For both the Flanker Task scans and the resting-state scan we removed signal associated with white matter, cerebrospinal fluid, and six motion parameters. In the resting-state scan analyses we also removed signal associated with a global time series, generated by averaging across all voxels in the brain. The 4-D residual time-series obtained after removing the nuisance covariates were used for the subsequent subject-level analyses.

Flanker Task

Individual Task Analysis—We performed a multiple regression analysis in which we regressed each participant's 4-D Flanker Task residuals volume on four task regressors coding for correct congruent trials, correct incongruent trials, errors across all trials, as well as a block regressor (which coded for task block). This analysis produced participant-level maps of all voxels exhibiting task-related activation and deactivation in the congruent (Congruent > Baseline) or incongruent trials (Incongruent > Baseline), as well as those voxels exhibiting differential activity for congruent and incongruent trials (Incongruent > Congruent). Finally, we also calculated overall task-related activation and deactivation across congruent and incongruent trials (i.e., Congruent + Incongruent > Baseline).

Group-level Task Analysis—Group-level analyses were carried out using a repeated-measures mixed-effects model as implemented in FSL FLAME. Multiple comparisons were corrected at the cluster level using Gaussian random field theory (min $Z > 2.3$; cluster significance: $p < 0.05$, corrected). This group-level analysis produced thresholded Z-statistic maps of activations and deactivations associated with the congruent or incongruent trials of the Flanker Task, or the combination of both trial types. Direct voxel-wise condition comparisons produced thresholded Z-statistic maps of those voxels that showed significant trial-related differences in activation (i.e., congruent vs. incongruent trials).

Resting-State Functional Connectivity

Seed Description—We created six 5mm radius seed ROIs (containing 81 voxels) centered around the coordinates used by Fox and colleagues (2005) to describe a task-positive and a task-negative network. The regions used for defining the task-positive network were located in the intraparietal sulcus (IPS; -25, -57, 46), the middle temporal region (MT+, -45, -69, -2), and the right frontal eye field (FEF) region of the precentral sulcus (25, -13, 50). The task-negative seed ROIs were located in left lateral parietal cortex (LP, -45, -67, 36), medial prefrontal cortex (MPF, -1, 47, -4), and posterior cingulate/precuneus (PCC, -5, -49, 40).

Individual Seed-based RSFC Analysis—First, in order to ensure that RSFC estimates resulting from regression analyses represent partial correlations, a voxel-wise normalization was performed on each participant's 4-D residuals volume by dividing each voxel's time-series by its standard deviation (Kelly et al., 2009b). Second, we spatially normalized each participant's residuals volume by applying the previously computed transformation to MNI152 standard space. We then extracted the time-series for each seed from these data. Time-series were averaged across all voxels in each seed ROI. Using the extracted time-series we performed a multiple regression analysis for each participant and each ROI including the participant's residuals volume as input data. This analysis was implemented in FSL FLAME and produced participant-level correlation maps of all voxels that were positively or negatively correlated with the seed time-series. Finally, these participant-level correlation maps were converted to Z-value maps using Fisher's *r*-to-*z* transformation.

Group-level Seed-based RSFC Analysis—For each seed ROI, group-level RSFC analyses were carried out using a mixed-effects model as implemented in FSL FLAME. Multiple comparisons were corrected at the cluster level using Gaussian random field theory (min $Z > 2.3$; cluster significance: $p < 0.05$, corrected). These group-level analyses produced thresholded Z-statistic maps (i.e., "networks") of positive and negative RSFC for each seed ROI.

RSFC with the Default Mode and Task-Positive Networks—Based on the group-level connectivity maps for each of the six seed ROIs, we created two maps representing the default mode and task-positive resting-state networks using a similar approach to Fox and colleagues (Fox et al., 2005). Specifically, to create the task-positive map, we averaged the positive Z-statistic maps for the three task-positive seeds and the negative Z-statistic maps for the three default mode seeds. The converse was done to obtain the default mode map. After averaging, we thresholded the averaged maps so that they included only voxels that were significantly correlated with at least five of the six seed regions. To assess the relationship between a voxel's task-induced BOLD response and its connectivity with larger functional networks instead of confined seed regions (see Individual and Group-Level Seed-Based RSFC Analysis), we repeated the individual and group-level seed based analyses using these task-positive and default mode maps as seeds. Thus, instead of using 5mm spherical ROIs we extracted the mean time-series for the entire network map and repeated the individual and group-level multiple regression analyses. This resulted in individual and group-level Z-statistic maps that indicated

for each voxel in the brain the correlation of its BOLD time-series with either the mean default mode or task-positive network map time-series.

ICA-based RSFC Analysis—To confirm our results and their independence from the specific analytical approach (i.e., seed-based) used for calculating RSFC, we performed a follow-up analysis in which we applied ICA, a data-driven approach, to identify the default mode network (Damoiseaux et al.; Kiviniemi et al., 2003; Smith et al., 2009). First, we spatially transformed all participants' preprocessed resting-state scans into MNI152 standard space. Considering the capability of ICA to automatically separate physiological noise from signals of interest, we did not remove the nuisance signals from the preprocessed resting-state scans. Subsequently we employed ICA as implemented in the MELODIC toolbox in FSL to perform a temporally concatenated group ICA on all resting-state data. We constrained the number of independent components to 25 (Beckmann et al., 2005). After ICA decomposition we visually inspected all components and selected the component representing the default mode network (see Figure 5). Finally, using the dual regression approach (Filippini et al., 2009) we back-reconstructed each individual's default mode resting-state network map. As indicated, this ICA-based analysis was added to the current study to confirm the validity of our findings across different approaches for calculating RSFC strength. Here we focused on a single default mode ICA component. Future work will need to explore other components in order to fully assess the extent of the current approach.

Predicting BOLD Activity During the Flanker Task based on Resting State Functional Connectivity

To predict each voxel's BOLD response during the Flanker task based on that voxel's RSFC strength, we conducted a *voxel-matched* linear regression analysis for each voxel in the brain (see Figure 1 for a schematic). Specifically, we entered each voxel's RSFC strength with each seed or network map as a predictor in the regression model separately for each of the six seed ROIs, the task-positive, the default mode and the ICA default mode networks. Subsequently, the parameter estimates for the Flanker task of that same voxel were entered as dependent variables. This resulted in a unique linear regression model for each voxel in which RSFC predicted BOLD activity induced by the Flanker task (see Figure 1). Separate analyses were conducted for the Congruent + Incongruent > Baseline, Congruent > Baseline, Incongruent > Baseline, and Incongruent > Congruent parameter estimates. In practice, we first concatenated the participant-level RSFC maps for all 26 participants into a 26-volume 4-D image (1 volume/participant). Separately we concatenated the participant-level Flanker task parameter estimates of all participants into a similar 26-volume 4-D image. Next we assessed for each voxel in the brain whether there was a significant linear relationship between RSFC and task-induced activity across participants. This analysis produced, at each voxel, a regression coefficient corresponding to the correlation across the 26 participants between RSFC and task-induced activity at that voxel. These values were converted to Z-statistics and the resultant whole-brain Z-statistic maps were corrected for multiple comparisons at the cluster level using Gaussian random field theory ($Z > 2.3$; cluster significance: $p < 0.05$, corrected). Each thresholded map contained clusters of voxels that exhibited a significant linear relationship between their BOLD response measured during a given condition of the Flanker task and their RSFC strength with a given seed region or network.

Sorting of Significant Regions

For each of the regions that showed a significant relationship between RSFC and task-induced activity, we calculated the percentage of voxels that overlapped with either the task-positive or default mode resting-state networks. This was done using the group-level thresholded Z-statistic maps. In a final step, we quantified membership with the task-positive resting-state network specifically by computing a ratio indicating for each region the percentage of voxels

that were part of the task-positive network, relative to the total number of voxels in that region that were part of either of the two resting-state networks (ratio = [overlap with task-positive network / (overlap with task-positive network + overlap with default mode network)]). For each of the regions that showed a significant relationship between RSFC and task-induced activity, we also calculated the percentage of voxels that overlapped with either significant task-induced activation or deactivation separately, as indicated by the group-level Z-statistic maps.

Results

RSFC Strength Predicts Task-induced Activity

At each voxel in the brain, regression analyses assessed the relationship between task-induced BOLD responses and RSFC with each of the six seed ROIs (see Supplementary Figure 4 for results with a seed ROI located in ACC). For each seed, RSFC significantly predicted overall task-induced brain activity (Congruent + Incongruent > Baseline) in a number of brain regions (see Figure 2). The direction of the relationship, i.e., positive or negative, depended on the specific network membership of each seed. Specifically, consistent with our hypotheses, RSFC with the three task-positive seeds was directly related to task-induced activity. Greater *positive* connectivity with the seed region was associated with higher neural activity during task performance. Among these regions were middle temporal gyrus, lateral occipital cortex, dorsal and ventral anterior cingulate cortex, posterior cingulate cortex, precentral sulcus, frontal eye fields, superior, middle and inferior frontal gyrus, frontal pole, and insula. In contrast, regression analyses with the three default mode seed ROIs identified many of the same regions, though showing the opposite relationship. In particular, greater *negative* connectivity with the seed region predicted higher neural activity during task performance.

Beyond the level of the individual seed ROIs, regression analyses using RSFC with the task-positive network map similarly identified a number of brain regions where greater *positive* connectivity with the task-positive network map was associated with higher neural activity during task performance (see Figures 3 and 4). The location of these regions was consistent with the location of the regions found for the separate default mode seed ROI analyses. Kendall's W indexing spatial concordance between the resulting statistical (Z-score) maps for the task-positive and the default mode analyses was 0.70 indicating high concordance. Of the significant voxels obtained for the default mode analysis, 30% were also significant for the task-positive analyses. The percentage of overlapping voxels increased to 53% when the converse analysis was conducted (task-positive voxels that were also significant for default mode analyses), indicating that overall fewer voxels were uniquely significant for the task-positive seed ROI analyses. Analogous to the results for the individual default mode seed ROIs, greater *negative* connectivity with the default mode network map in its entirety was associated with higher neural activity during task performance (see Figures 3 and 4).

Across all analyses, only a few regions did not conform to the directionality of the relationships between RSFC and task-induced activity generally observed for the regions associated with that particular seed or network. These regions were primarily located within areas involved in the ventral processing stream – bilateral occipital poles, right intra-calcarine sulcus, left thalamus and right putamen.

Confirmation of Results Using ICA-derived Default Mode Network

To verify that our results were not specific to the seed-based functional connectivity analyses we employed, we repeated the voxel-matched regression analyses using RSFC obtained through dual-regression with the default mode ICA component. Similar to the results obtained using the seed-based approach, the regression analyses using the ICA-derived default mode

component identified a number of regions showing an inverse relationship between RSFC and overall task-induced activity (Congruent + Incongruent > Baseline) (see Figures 4 and 5). In these regions a greater *negative* association with the default mode component was associated with higher overall task-induced activity. Although the directionality of the relationship between RSFC and task-induced activity was the same for the ICA-derived and the seed-based default mode network, limited overlap existed in the location of the clusters showing a significant relationship (see Supplementary Figure 5; only 11% of the significant voxels found for the ICA-derived network were also significant for the seed-based default mode network; Kendall's W between the resulting statistical (Z-score) maps for seed-based and ICA-derived default mode network analyses was 0.53 [moderate concordance]).

Characterization of Significant Regions: Transition Zones

Across our analyses, regions exhibiting a significant relationship between RSFC strength and overall task-induced activity (Congruent + Incongruent > Baseline) were predominantly located within the task-positive resting-state network or in *transition zones* located between the default mode and task-positive networks (see Figures 2, 3 and 5). We observed that these transition zones are regions that were not consistently connected with either the default mode or task-positive resting-state networks. Instead, they reflect variability in network boundaries across participants. In those regions, task-induced neural activity was positively correlated across participants with the region's membership in the task-positive network. Participants showing greater expansion of the task-positive network into a given transition zone also showed higher task-induced neural activity in that region (see Figure 6). Finally, most regions that exhibited a significant task/RSFC relationship overlapped at least to some extent with areas of significant task-induced activation (see Figures 2, 3, and 5). Similar to the transition zones for the RSFC networks, most of these regions were located near the boundaries of the task-induced activation and deactivation maps. Only a few regions overlapped with significant task-induced deactivation.

Verification of Results for Specific Trial Types and Congruency Effect

To verify that a specific trial type did not drive our results, we repeated our analyses using RSFC to predict task activity induced by the congruent or incongruent trials of the flanker task (Congruent > Baseline or Incongruent > Baseline). These analyses revealed mostly identical regions and relationships as the analyses using overall task-induced activity (Congruent + Incongruent > Baseline), confirming that our results were not trial-type specific (see Supplementary Figure 1). Specifically, between 37% and 57% of the voxels that were significant for the Congruent > Baseline analyses were also significant for the Incongruent > Baseline analyses. Lower percentages were found when comparing Incongruent > Baseline to Congruent > Baseline, indicating that more uniquely significant voxels were found for the Incongruent > Baseline analyses. Kendall's W values ranged between 0.70 and 0.76 (high concordance). In addition, between 67% and 86% of the voxels that were significant for the Congruent > Baseline or Incongruent > Baseline analyses were also significant for the Congruent + Incongruent > Baseline analysis. The spatial concordance between the statistical (Z-score) maps obtained for each of the individual trial types (Congruent or Incongruent > Baseline) and the analyses using overall task-induced activity (Congruent + Incongruent > Baseline) was very high, with Kendall's W values between .88 and .92 (maximum=1.0).

Finally, we examined the extent to which RSFC could predict inter-individual differences in the brain's response to incongruent trials when directly compared to congruent trials rather than to baseline. Regression analyses using RSFC to predict task-induced activity associated with the congruency effect (Incongruent > Congruent) identified a smaller number of significant regions, showing minimal overlap with the regions found for overall task-induced activity (see Figure 7). Across the seed-based, seed-based networks, and ICA-derived network

analyses the highest percentage of overlapping voxels between the sparse results obtained for Incongruent > Congruent and Congruent + Incongruent > Baseline was only 10%. Despite this low degree of overlap, the results resembled those for overall task-induced activity, with a number of regions located between the default mode and task-positive network or between overall or trial specific task activation and deactivation regions. In contrast to the results for overall task-induced activity, however, several regions were located within areas of significant task-induced activation or deactivation. These regions included ventromedial prefrontal cortex, precuneus, right insula, right inferior-frontal junction and right lateral occipital cortex for analyses examining the relationship with RSFC based on the default mode network map seed. For analyses with the task-positive network map, the same right-lateralized regions were found along with a region in left superior frontal junction.

Notwithstanding differences in the specific location of significant regions detected using the congruency effect (i.e., Incongruent > Congruent) as opposed to overall task-induced activity, we confirmed that greater positive connectivity with the task-positive seeds or task-positive network map predicted higher task-induced neural activity. Similarly greater negative association with the default mode seeds or the corresponding network map again predicted higher task-induced neural activity (see Figure 4). These relationships were mainly driven by an increase in task-induced activity during incongruent trials in participants who showed greater RSFC of the particular significant region to the task-positive network (see Supplementary Figure 2). Conversely, participants showing greater negative association of a region with the default mode network exhibited greater task-induced decreases in neural activity during incongruent trials. In both cases, task-induced activity during congruent trials remained mostly stable across participants (see Supplementary Figure 2).

Accounting for Inter-individual Differences in Structure

Considering the functional transition zones and their associated variability across participants, an obvious question is the extent to which they merely reflect underlying structural variability. We explored this question by repeating our voxel-matched analyses while accounting for voxel-based morphometry measures of gray matter density (Ashburner and Friston, 2000). At each voxel we used gray matter densities obtained from the segmentation of each participant's structural scan using FSL FAST. In other words, the model at each voxel now included both RSFC and gray matter density as predictors and task-induced activity as the dependent variable. Accounting for gray matter density did not change results appreciably, indicating that structural variability is not driving the RSFC/task-induced activity relationships observed in the present study (see Supplementary Figure 3).

Behavioral Results

Results for the behavioral parameters obtained during the Flanker task are described in full elsewhere (Kelly et al., 2008). No significant relationships were found between the current results and any of the behavioral parameters (i.e., mean reaction time, coefficient of variation).

Discussion

In the present work we examined inter-individual differences in the magnitude of a region's task-induced activity in relation to inter-individual differences in the same region's resting-state functional connectivity (RSFC) properties. For a number of regions, higher task-induced increases in neural activity during a standard selective attention task were significantly related to stronger *positive* connectivity with the task-positive network. Higher task-induced increases in neural activity were also related to greater *negative* connectivity with the default mode network. In other words, the more strongly connected a region is with the task-positive network or the more segregated a region is from the default mode network, the higher its task-induced

activity. Using ICA, we confirmed that our findings regarding the default mode network did not depend upon a seed-based approach for calculating a voxel's RSFC strength. The particular task contrast used (Congruent + Incongruent > Baseline, Incongruent > Congruent) determined the specific regions where inter-individual differences in task-induced activity could be explained by that region's RSFC properties. Both contrasts revealed several *transition zones* between the default mode and task-positive networks. In these transition zones inter-individual differences in task-induced activity were related to inter-individual differences in the relative dominance of one network or the other.

At least for the regions identified in the present work, a common mechanism appears to govern both inter-individual differences in task-induced activity as well as inter-individual differences in RSFC strength. The presence of significant relationships between a region's RSFC properties and task activation across participants suggests that at least some part of the inter-individual variability in the BOLD response induced by a particular task is intrinsically represented in the brain. Moreover, we can use fMRI during rest to quantify inter-individual differences in these intrinsic representations. The stability of inter-individual differences in the spatial extent of RSFC networks, even over a 5-11 month period (Shehzad et al., 2009), further supports the hypothesis that part of the BOLD response is intrinsically represented in the brain. These results complement prior findings that accounting for intrinsic low frequency fluctuations dramatically enhances the signal-to-noise ratio of task-based analyses (Fox et al., 2006) and that such intrinsic fluctuations are related to behavioral variability within (Fox et al., 2007) and across participants (Kelly et al., 2008).

Of course, while standard task-based fMRI analyses highlight the relatively invariant aspects of the BOLD response to a stimulus or behavioral response by detecting neural activations that are consistent across participants, the BOLD signal is notoriously variable. This variability likely depends on multiple factors including highly specific stimulus characteristics, participant emotional or attentional state (Kay et al., 2008; Schultz and Lennert, 2009; Urry et al., 2009), or current physiological state (e.g., menstrual cycle for females, caffeine, hunger) (Amin et al., 2006; Haase et al., 2009; Protopopescu et al., 2005; Siep et al., 2009 hunger). Similarly, the dynamic aspects of RSFC have begun to be observed (Chang and Glover, 2009). Modulations in RSFC were found after learning (Albert et al., 2009; Lewis et al., 2009; Xiong et al., 2009), in relation to specific task demands (Barnes et al., 2009; Fransson, 2006; Hampson et al., 2006; Hasson et al., 2009; Kelly et al., 2008), or conscious and emotional states (Greicius et al., 2008; Harrison et al., 2008; Horovitz et al., 2008).

Our most surprising observation was the identification of *transition zones* that appear to index inter-individual variability in network extent across task and rest. Participants with greater task-positive network dominance in a particular region during rest showed greater task-induced neural activations in that region, while participants with default mode network dominance in that region during rest did not show such activations. This result resonates with the recent finding of sharp transitions in functional connectivity patterns across regions (Cohen et al., 2008). Cohen et al. (2008) also noted the concordance of the transition regions and borders of activations observed in functional activation studies. Consistent with Cohen et al.'s observation linking the boundaries of task-based activations and functional regions defined using RSFC, our analyses suggest that inter-individual differences in the spatial extent of task-induced activations are governed by the same mechanisms that undergird RSFC networks (Steyn-Ross et al., 2009). This finding further supports the potential utility of resting-state approaches to study the developing (< 18 year old) and aging (> 65 year old) brain, which are both characterized by greater spatial extent of activation and RSFC (Andrews-Hanna et al.; Durston et al., 2006; Emery et al., 2008; Fair et al., 2008; Fair et al., 2007; Kelly et al., 2009a). These observations may also provide candidate biomarkers for clinical populations in which

pathological processes appear to impact the spatial extent of task-induced activations (e.g., autism, ADHD) (Durston et al., 2003; Mostofsky et al., 2006).

We considered the possibility that inter-individual differences in gyral structure and/or inaccuracies introduced by registration of each individual's structural scan to the MNI152 template might have contributed to our results (Cohen et al., 2008). Such concern is especially notable given our highlighting the presence of *transition zones*, which may be most sensitive to differences in structure and/or registration errors. However, taking into account inter-individual differences in gray matter density at each voxel did not impact our results appreciably, underlining the robustness of our results. Still, given that our understanding of structure/function relationships in resting-state fMRI is only just emerging, this issue merits further examination (Greicius et al., 2009; Hagmann et al., 2008; Honey et al., 2009; Skudlarski et al., 2008; van den Heuvel et al., 2009).

Additional concerns may arise regarding the specificity of our results to the default mode and task-positive network seed ROIs. We selected these networks because of their widespread reproducibility and the high degree of overlap between their component regions and those previously found to be activated or deactivated during performance of attentionally demanding tasks (Greicius and Menon, 2004; Smith et al., 2009; Thomason et al., 2008; Toro et al., 2008). The ability to identify the default mode network through multiple methods made it an especially appealing first choice. Future work investigating the relationship between RSFC based on regions specifically activated by the task being examined is warranted.

The value of attending to transition zones between functional networks was supported by a recent observation of lower informant ratings of autistic traits in participants for whom a mid-insula transition zone was dominated by the RSFC properties of the ventral anterior insula (Di Martino et al., 2009). In the present data, we did not find significant associations between either RSFC or task-induced activity and behavioral measures of task performance (mean response time or coefficient of variation) in the regions that showed a significant relationship between RSFC and task-induced activity. By contrast, in these same data, Kelly et al. (2008) observed significant relationships between the coefficient of variation and the strength of the anti-correlation between the default mode and task positive networks. Future work including denser response sets (i.e., more than 48 trials) will be needed to address the potential behavioral significance of inter-individual differences in the neural properties of transition zones between functional systems.

Beyond the transition zones detected in relation to overall task-induced activity (Congruent + Incongruent > Baseline), we found that the BOLD response associated with the congruency effect (Incongruent > Congruent) was also predicted by RSFC. Unlike the distributed pattern of overall task-induced activity, which encompassed large portions of occipital, parietal, insular and sensorimotor cortices, areas exhibiting significantly greater activation for incongruent relative to congruent trials were restricted to the intraparietal sulcus and temporo-occipital cortex bilaterally, as well as right inferior frontal cortex (see Supplementary Figure 6). In contrast to the areas exhibiting a relationship between RSFC and overall task-induced activity, several regions that showed a relationship between RSFC and the congruency effect were located within the resting-state networks, rather than in transition zones between networks. Similarly, these regions did not show consistent activation across participants for the Incongruent > Congruent task contrast, but were part of the overall pattern of task-induced activity (i.e., Congruent + Incongruent > Baseline; see Figure 7). Interestingly, the magnitude of the congruency effect within these regions appeared to depend primarily on RSFC membership. Greater positive connectivity with the task-positive network predicted a larger difference between activation for incongruent relative to congruent trials. This relationship was mainly driven by differences during the incongruent trials (see Supplementary Figure 2),

suggesting that intrinsic BOLD activity may have greater significance for task-induced activation when processing requirements are higher (as they are for incongruent trials), than when they are lower. Since this study only included a slow event-related version of the Flanker task, future work will have to assess whether our results generalize to other task paradigms.

Finally, we note that our results for the FEF seed differed somewhat from those for the two other task-positive seeds, IPS and MT+ (see Figure 2). Specifically half of the clusters obtained for FEF showed the opposite relationship to what we hypothesized for task-positive network seeds. In these clusters greater negative connectivity was associated with higher neural activity. This discrepancy might be related to differences in the resting-state connectivity maps obtained for the FEF seed compared to those obtained with the other task-positive seeds. For instance, the FEF-based task-positive network misses the temporal-occipital positive connectivity observed for IPS and MT+. On the other hand there is greater connectivity with the medial wall for the FEF seed (seen on the top part of the flat surface maps in Figure 2). As such it is possible that FEF might represent a locus of interaction between the default mode and task-positive resting-state networks.

Summary

Increased interest in resting-state fMRI has focused attention on the intrinsic properties of the brain. Here we were able to link functional connectivity measures obtained during rest to fMRI measures obtained during task performance. Using voxel-matched regression analyses, we showed that across participants a region's intrinsic activity as measured during rest predicted that same region's activity induced by a Flanker task. Building on two well-characterized RSFC networks, this work represents an initial effort in coupling resting-state measures to task-induced brain activity. Further research is needed to fully assess the potential of resting-state fMRI to complement task-based imaging research and to provide an alternative functional imaging approach for clinical and developmental applications.

Supplementary Material

Refer to Web version on PubMed Central for supplementary material.

Acknowledgments

The authors thank all participants for their cooperation, and Amy Roy, Maki Koyama, and Jonathan Adelstein for helpful comments on earlier versions of this manuscript. This research was partially supported by grants from NIMH (R01MH083246), Autism Speaks, the Stavros Niarchos Foundation, the Leon Levy Foundation, and gifts from Joseph P. Healy, Linda and Richard Schaps, Jill and Bob Smith, and the endowment provided by Phyllis Green and Randolph Cōwen.

References

Albert NB, Robertson EM, Miall RC. The resting human brain and motor learning. Curr Biol 2009;19:1023–1027. [PubMed: 19427210]

Amin Z, Epperson CN, Constable RT, Canli T. Effects of estrogen variation on neural correlates of emotional response inhibition. Neuroimage 2006;32:457–464. [PubMed: 16644236]

Andersson, JLR.; Jenkinson, M.; Smith, SM. TR07JA2 : Non-linear registration, aka Spatial normalisation. FMRIB Analysis Group Technical Reports. 2007. http://www.fmrib.ox.ac.uk/analysis/techrep/

Andrews-Hanna JR, Snyder AZ, Vincent JL, Lustig C, Head D, Raichle ME, Buckner RL. Disruption of large-scale brain systems in advanced aging. Neuron 2007;56:924–935. [PubMed: 18054866]

Ashburner J, Friston KJ. Voxel-based morphometry--the methods. Neuroimage 2000;11:805–821. [PubMed: 10860804]

Barnes A, Bullmore ET, Suckling J. Endogenous human brain dynamics recover slowly following cognitive effort. PLoS One 2009;4:e6626. [PubMed: 19680553]

Beckmann CF, De Luca M, Devlin JT, Smith SM. Investigations into resting-state connectivity using independent component analysis. Philos Trans R Soc Lond B Biol Sci 2005;360:1001–1013. [PubMed: 16087444]

Biswal B, Yetkin FZ, Haughton VM, Hyde JS. Functional connectivity in the motor cortex of resting human brain using echo-planar MRI. Magn Reson Med 1995;34:537–541. [PubMed: 8524021]

Brown JW. Conflict effects without conflict in anterior cingulate cortex: multiple response effects and context specific representations. Neuroimage 2009;47:334–341. [PubMed: 19375509]

Bunge SA, Hazeltine E, Scanlon MD, Rosen AC, Gabrieli JD. Dissociable contributions of prefrontal and parietal cortices to response selection. Neuroimage 2002;17:1562–1571. [PubMed: 12414294]

Chang C, Glover GH. Time-frequency dynamics of resting-state brain connectivity measured with fMRI. Neuroimage. 2009 epub ahead of print.

Cohen AL, Fair DA, Dosenbach NU, Miezin FM, Dierker D, Van Essen DC, Schlaggar BL, Petersen SE. Defining functional areas in individual human brains using resting functional connectivity MRI. Neuroimage 2008;41:45–57. [PubMed: 18367410]

Cox RW. AFNI: software for analysis and visualization of functional magnetic resonance neuroimages. Comput Biomed Res 1996;29:162–173. [PubMed: 8812068]

Damoiseaux JS, Rombouts SA, Barkhof F, Scheltens P, Stam CJ, Smith SM, Beckmann CF. Consistent resting-state networks across healthy subjects. Proc Natl Acad Sci U S A 2006;103:13848–13853. [PubMed: 16945915]

Di Martino A, Ross K, Uddin LQ, Sklar AB, Castellanos FX, Milham MP. Functional brain correlates of social and nonsocial processes in autism spectrum disorders: an activation likelihood estimation meta-analysis. Biol Psychiatry 2009;65:63–74. [PubMed: 18996505]

Dosenbach NUF, Fair DA, Miezin FM, Cohen AL, Wenger KK, Dosenbach RAT, Fox MD, Snyder AZ, Vincent JL, Raichle ME, Schlaggar BL, Petersen SE. Distinct Brain Networks for Adaptive and Stable Task Control in Humans. Proc Natl Acad Sci U S A 2007;104:11073–11078. [PubMed: 17576922]

Durston S, Davidson MC, Tottenham N, Galvan A, Spicer J, Fossella JA, Casey BJ. A shift from diffuse to focal cortical activity with development. Dev Sci 2006;9:1–8. [PubMed: 16445387]

Durston S, Tottenham NT, Thomas KM, Davidson MC, Eigsti IM, Yang Y, Ulug AM, Casey BJ. Differential patterns of striatal activation in young children with and without ADHD. Biol Psychiatry 2003;53:871–878. [PubMed: 12742674]

Emery L, Heaven TJ, Paxton JL, Braver TS. Age-related changes in neural activity during performance matched working memory manipulation. Neuroimage 2008;42:1577–1586. [PubMed: 18634891]

Fair DA, Cohen AL, Dosenbach NU, Church JA, Miezin FM, Barch DM, Raichle ME, Petersen SE, Schlaggar BL. The maturing architecture of the brain's default network. Proc Natl Acad Sci U S A 2008;105:4028–4032. [PubMed: 18322013]

Fair DA, Dosenbach NUF, Church JA, Cohen AL, Brahmbhatt S, Miezin FM, Barch DM, Raichle ME, Petersen SE, Schlaggar BL. Development of distinct control networks through segregation and integration. Proc Natl Acad Sci U S A 2007;104:13507–13512. [PubMed: 17679691]

Filippini N, MacIntosh BJ, Hough MG, Goodwin GM, Frisoni GB, Smith SM, Matthews PM, Beckmann CF, Mackay CE. Distinct patterns of brain activity in young carriers of the APOE-epsilon4 allele. Proc Natl Acad Sci U S A 2009;106:7209–7214. [PubMed: 19357304]

Fox MD, Raichle ME. Spontaneous fluctuations in brain activity observed with functional magnetic resonance imaging. Nat Rev Neurosci 2007;8:700–711. [PubMed: 17704812]

Fox MD, Snyder AZ, Vincent JL, Corbetta M, Van Essen DC, Raichle ME. The human brain is intrinsically organized into dynamic, anticorrelated functional networks. Proc Natl Acad Sci U S A 2005;102:9673–9678. [PubMed: 15976020]

Fox MD, Snyder AZ, Vincent JL, Raichle ME. Intrinsic fluctuations within cortical systems account for intertrial variability in human behavior. Neuron 2007;56:171–184. [PubMed: 17920023]

Fox MD, Snyder AZ, Zacks JM, Raichle ME. Coherent spontaneous activity accounts for trial-to-trial variability in human evoked brain responses. Nat Neurosci 2006;9:23–25. [PubMed: 16341210]

Fransson P. How default is the default mode of brain function? Further evidence from intrinsic BOLD signal fluctuations. Neuropsychologia 2006;44:2836–2845. [PubMed: 16879844]

Greicius MD, Kiviniemi V, Tervonen O, Vainionpaa V, Alahuhta S, Reiss AL, Menon V. Persistent default-mode network connectivity during light sedation. Hum Brain Mapp 2008;29:839–847. [PubMed: 18219620]

Greicius MD, Krasnow B, Reiss AL, Menon V. Functional connectivity in the resting brain: a network analysis of the default mode hypothesis. Proc Natl Acad Sci U S A 2003;100:253–258. [PubMed: 12506194]

Greicius MD, Menon V. Default-mode activity during a passive sensory task: uncoupled from deactivation but impacting activation. J Cogn Neurosci 2004;16:1484–1492. [PubMed: 15601513]

Greicius MD, Supekar K, Menon V, Dougherty RF. Resting-state functional connectivity reflects structural connectivity in the default mode network. Cereb Cortex 2009;19:72–78. [PubMed: 18403396]

Haase L, Cerf-Ducastel B, Murphy C. Cortical activation in response to pure taste stimuli during the physiological states of hunger and satiety. Neuroimage 2009;44:1008–1021. [PubMed: 19007893]

Hagmann P, Cammoun L, Gigandet X, Meuli R, Honey CJ, Wedeen VJ, Sporns O. Mapping the structural core of human cerebral cortex. PLoS Biol 2008;6:e159. [PubMed: 18597554]

Hampson M, Driesen NR, Skudlarski P, Gore JC, Constable RT. Brain connectivity related to working memory performance. J Neurosci 2006;26:13338–13343. [PubMed: 17182784]

Harrison BJ, Pujol J, Ortiz H, Fornito A, Pantelis C, Yucel M. Modulation of brain resting-state networks by sad mood induction. PLoS One 2008;3:e1794. [PubMed: 18350136]

Hasson U, Nusbaum HC, Small SL. Task-dependent organization of brain regions active during rest. Proc Natl Acad Sci U S A 2009;106:10841–10846. [PubMed: 19541656]

Honey CJ, Sporns O, Cammoun L, Gigandet X, Thiran JP, Meuli R, Hagmann P. Predicting human resting-state functional connectivity from structural connectivity. Proc Natl Acad Sci U S A 2009;106:2035–2040. [PubMed: 19188601]

Horovitz SG, Fukunaga M, de Zwart JA, van Gelderen P, Fulton SC, Balkin TJ, Duyn JH. Low frequency BOLD fluctuations during resting wakefulness and light sleep: a simultaneous EEG-fMRI study. Hum Brain Mapp 2008;29:671–682. [PubMed: 17598166]

Jenkinson M, Bannister PR, Brady JM, Smith SM. Improved optimisation for the robust and accurate linear registration and motion correction of brain images. Neuroimage 2002;17:825–841. [PubMed: 12377157]

Jenkinson M, Smith SM. A global optimisation method for robust affine registration of brain images. Med Image Anal 2001;5:143–156. [PubMed: 11516708]

Kay KN, Naselaris T, Prenger RJ, Gallant JL. Identifying natural images from human brain activity. Nature 2008;452:352–355. [PubMed: 18322462]

Kelly AM, Di Martino A, Uddin LQ, Shehzad Z, Gee DG, Reiss PT, Margulies DS, Castellanos FX, Milham MP. Development of anterior cingulate functional connectivity from late childhood to early adulthood. Cereb Cortex 2009a;19:640–657. [PubMed: 18653667]

Kelly AM, Uddin LQ, Biswal BB, Castellanos FX, Milham MP. Competition between functional brain networks mediates behavioral variability. Neuroimage 2008;39:527–537. [PubMed: 17919929]

Kelly C, de Zubicaray G, Di Martino A, Copland DA, Reiss PT, Klein DF, Castellanos FX, Milham MP, McMahon K. L-dopa modulates functional connectivity in striatal cognitive and motor networks: a double-blind placebo-controlled study. J Neurosci 2009b;29:7364–7378. [PubMed: 19494158]

Kiviniemi V, Kantola JH, Jauhiainen J, Hyvarinen A, Tervonen O. Independent component analysis of nondeterministic fMRI signal sources. Neuroimage 2003;19:253–260. [PubMed: 12814576]

Kiviniemi V, Starck T, Remes J, Long X, Nikkinen J, Haapea M, Veijola J, Moilanen I, Isohanni M, Zang YF, Tervonen O. Functional segmentation of the brain cortex using high model order group PICA. Hum Brain Mapp. 2009 Epub ahead of print.

Lewis CM, Baldassarre A, Committeri G, Romani GL, Corbetta M. Learning sculpts the spontaneous activity of the resting human brain. Proc Natl Acad Sci U S A 2009;106:17558–17563. [PubMed: 19805061]

Margulies DS, Kelly AMC, Uddin LQ, Biswal BB, Castellanos FX, Milham MP. Mapping the Functional Connectivity of Anterior Cingulate Cortex. Neuroimage 2007;37:579–588. [PubMed: 17604651]

Mostofsky SH, Rimrodt SL, Schafer JG, Boyce A, Goldberg MC, Pekar JJ, Denckla MB. Atypical motor and sensory cortex activation in attention-deficit/hyperactivity disorder: a functional magnetic resonance imaging study of simple sequential finger tapping. Biol Psychiatry 2006;59:48–56. [PubMed: 16139806]

Ochsner KN, Hughes B, Robertson ER, Cooper JC, Gabrieli JD. Neural systems supporting the control of affective and cognitive conflicts. J Cogn Neurosci 2009;21:1842–1855. [PubMed: 18823233]

Protopopescu X, Pan H, Altemus M, Tuescher O, Polanecsky M, McEwen B, Silbersweig D, Stern E. Orbitofrontal cortex activity related to emotional processing changes across the menstrual cycle. Proc Natl Acad Sci U S A 2005;102:16060–16065. [PubMed: 16247013]

Schultz J, Lennert T. BOLD signal in intraparietal sulcus covaries with magnitude of implicitly driven attention shifts. Neuroimage 2009;45:1314–1328. [PubMed: 19349243]

Shehzad Z, Kelly AM, Reiss PT, Gee DG, Gotimer K, Uddin LQ, Lee SH, Margulies DS, Roy AK, Biswal BB, Petkova E, Castellanos FX, Milham MP. The resting brain: unconstrained yet reliable. Cereb Cortex 2009;19:2209–2229. [PubMed: 19221144]

Siep N, Roefs A, Roebroeck A, Havermans R, Bonte ML, Jansen A. Hunger is the best spice: an fMRI study of the effects of attention, hunger and calorie content on food reward processing in the amygdala and orbitofrontal cortex. Behav Brain Res 2009;198:149–158. [PubMed: 19028527]

Skudlarski P, Jagannathan K, Calhoun VD, Hampson M, Skudlarska BA, Pearlson G. Measuring brain connectivity: diffusion tensor imaging validates resting state temporal correlations. Neuroimage 2008;43:554–561. [PubMed: 18771736]

Smith SM, Fox PT, Miller KL, Glahn DC, Fox PM, Mackay CE, Filippini N, Watkins KE, Toro R, Laird AR, Beckmann CF. Correspondence of the brain's functional architecture during activation and rest. Proc Natl Acad Sci U S A 2009;106:13040–13045. [PubMed: 19620724]

Steyn-Ross ML, Steyn-Ross DA, Wilson MT, Sleigh JW. Modeling brain activation patterns for the default and cognitive states. Neuroimage 2009;45:298–311. [PubMed: 19121401]

Thomason ME, Chang CE, Glover GH, Gabrieli JD, Greicius MD, Gotlib IH. Default-mode function and task-induced deactivation have overlapping brain substrates in children. Neuroimage 2008;41:1493–1503. [PubMed: 18482851]

Toro R, Fox PT, Paus T. Functional coactivation map of the human brain. Cereb Cortex 2008;18:2553–2559. [PubMed: 18296434]

Urry HL, van Reekum CM, Johnstone T, Davidson RJ. Individual differences in some (but not all) medial prefrontal regions reflect cognitive demand while regulating unpleasant emotion. Neuroimage 2009;47:852–863. [PubMed: 19486944]

van den Heuvel MP, Mandl RC, Kahn RS, Hulshoff Pol HE. Functionally linked resting-state networks reflect the underlying structural connectivity architecture of the human brain. Hum Brain Mapp 2009;30:3127–3141. [PubMed: 19235882]

Van Essen DC. A Population-Average, Landmark- and Surface-based (PALS) atlas of human cerebral cortex. Neuroimage 2005;28:635–662. [PubMed: 16172003]

Vincent JL, Patel GH, Fox MD, Snyder AZ, Baker JT, Van Essen DC, Zempel JM, Snyder LH, Corbetta M, Raichle ME. Intrinsic functional architecture in the anaesthetized monkey brain. Nature 2007;447:83–86. [PubMed: 17476267]

Xiong J, Ma L, Wang B, Narayana S, Duff EP, Egan GF, Fox PT. Long-term motor training induced changes in regional cerebral blood flow in both task and resting states. Neuroimage 2009;45:75–82. [PubMed: 19100845]

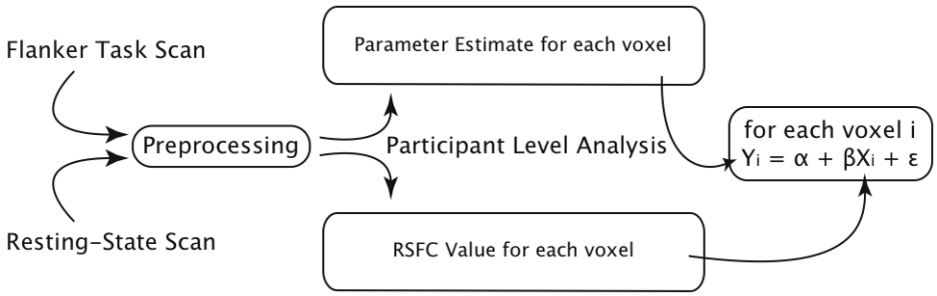

Figure 1. Path schematic for analyses

After preprocessing and appropriate participant level analyses, the task-induced parameter estimates and specific RSFC strengths were, for each voxel, combined in a unique, voxel-matched regression model. Across participants, RSFC was used to predict the task-induced BOLD-response.

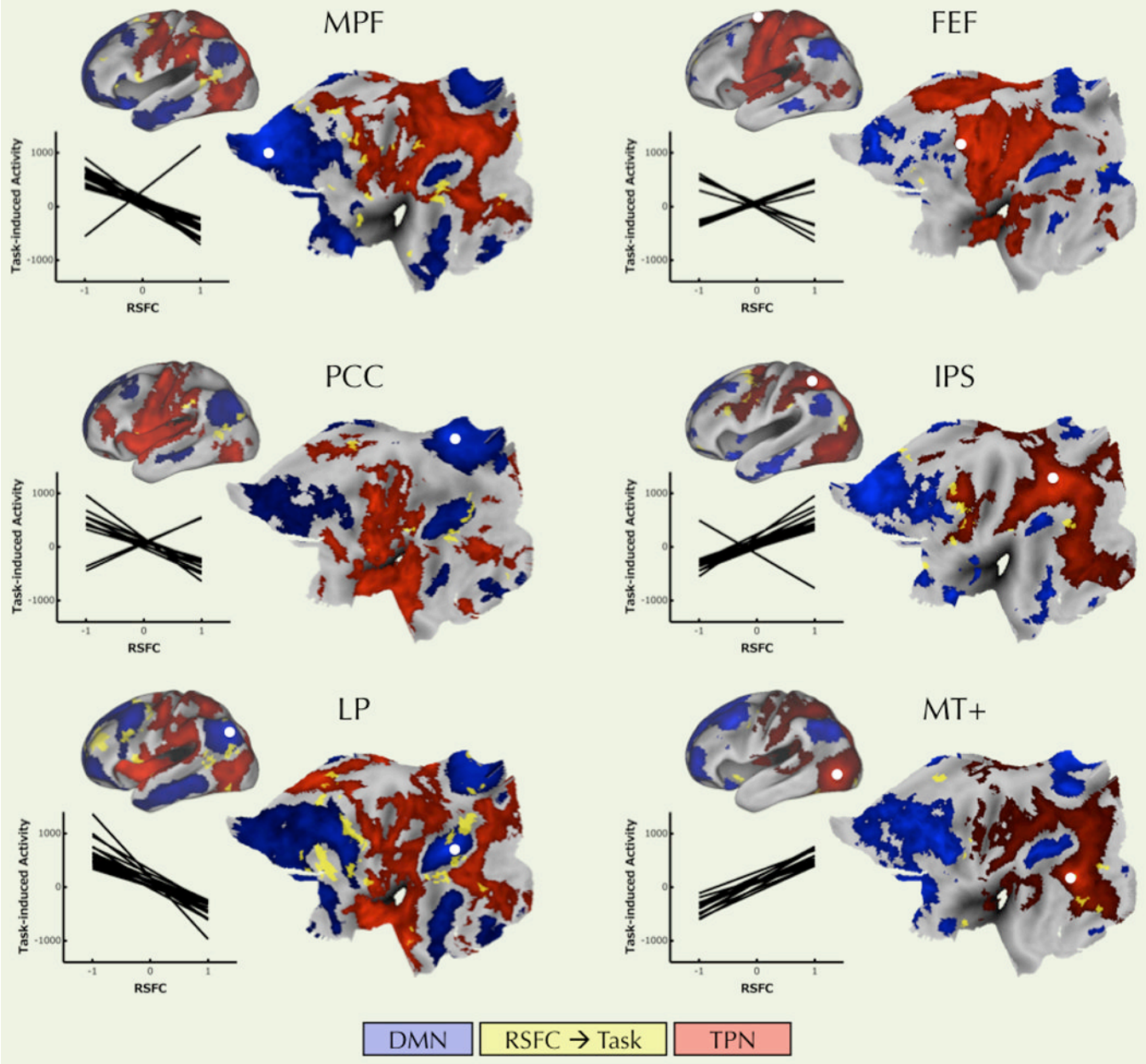

Figure 2. RSFC with each of the six seeds significantly predicted overall task-induced activity

For each of the three default mode seed ROIs (left column), greater negative connectivity with the seed predicted higher overall task-induced activity (Congruent + Incongruent > Baseline). For each of the three task-positive seed ROIs (right column), greater positive connectivity with the seed also predicted higher overall task-induced activity. Clusters showing a significant relationship between RSFC and overall task-induced activity are shown in yellow. White dots represent the location of the seed ROIs. Blue underlay shows the default mode network based on each particular seed ROI's RSFC. The red underlay shows the task-positive network based on each particular seed ROI's RSFC. In the inset graphs each line represents the linear relationship across participants between RSFC (X axis) and overall task-induced activity (Y axis) for each significant cluster. Only a few clusters, mostly for the FEF seed, showed a relationship between RSFC and overall task-induced activity opposite to the direction expected

for the specific seed. MPF: medial prefrontal cortex; FEF: frontal eye field, PCC: posterior cingulate cortex; IPS: intra parietal sulcus; MT+: middle temporal region. All statistical maps were corrected for multiple comparisons using Gaussian random field theory ($Z > 2.3$; $p < 0.05$, corrected). All surface maps were drawn on the PALS B-12 atlas (Van Essen, 2005) available in CARET. Transformation from MNI152 standard space to 711-2C CARET space was established using the FLIRT transformation included in CARET. Supplementary Figure 4 shows similar results using another seed located in the motor-related part of anterior cingulate cortex, ACC S1, as described by Margulies et al. (2007).

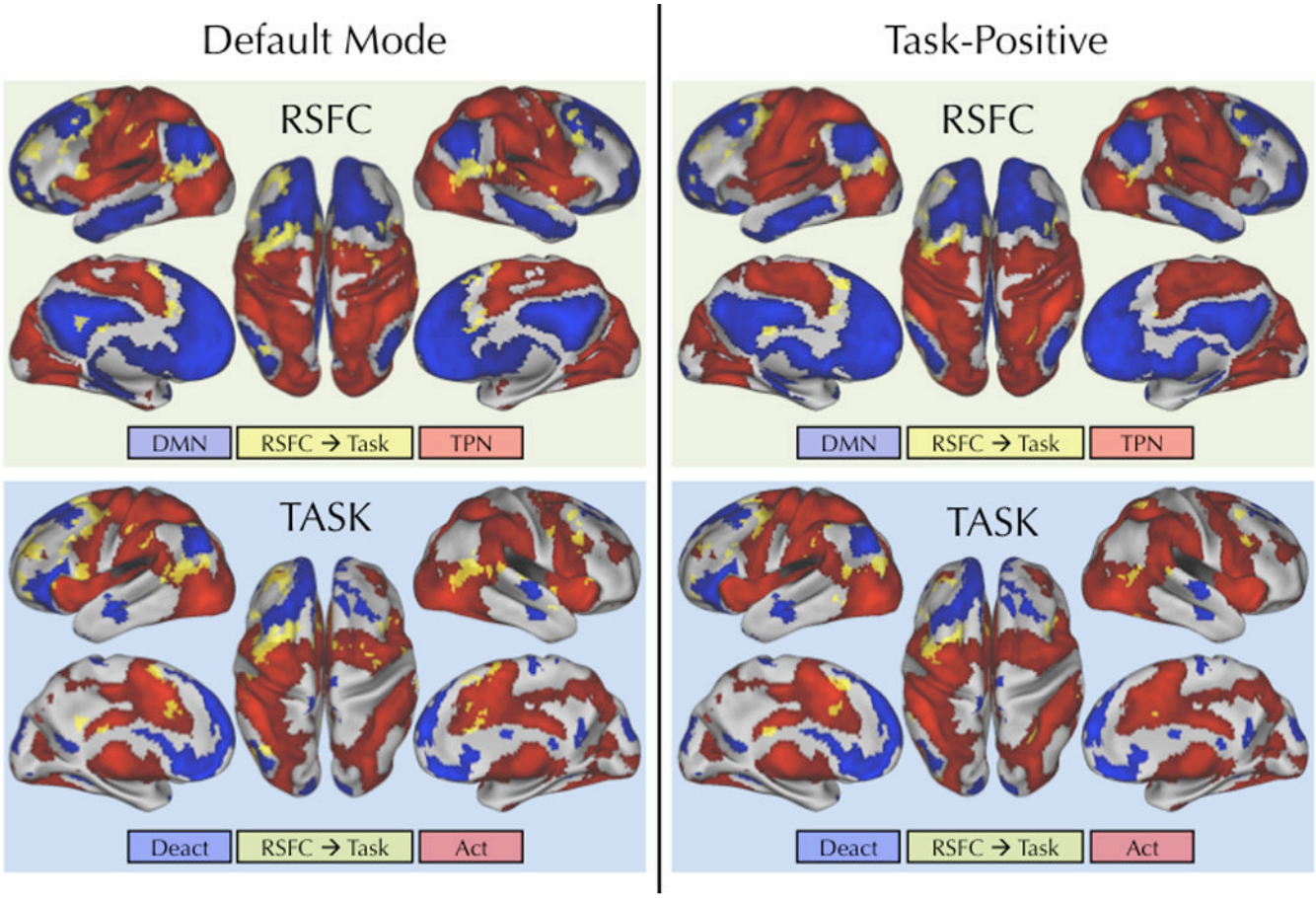

Figure 3. RSFC with the default mode or task-positive network maps significantly predicted overall task-induced activity

Figures in the top row illustrate the regions (yellow) showing a significant relationship between their RSFC with the default mode (left) or task-positive (right) resting state network maps and their overall task-induced activity (Congruent + Incongruent > Baseline). These regions are overlaid on the default mode (blue) and task-positive (red) resting-state networks. Bottom-row figures show the same significant regions (yellow) overlaid on overall task-induced activations (red) and deactivations (blue). Compared to the network maps derived for each individual seed ROI (see Figure 2), the current RSFC maps were obtained by calculating functional connectivity with a conjunction default mode or task-positive network map. A voxel was included in the conjunction map if it belonged to either the default mode or task-positive network for at least 5 of the 6 seed ROIs. Next, each conjunction map was used as a seed in a new functional connectivity analysis. DMN: default mode network; TPN: task positive network; Deact: task-related deactivations; Act: task-related activations. Statistical maps were corrected for multiple comparisons using Gaussian random field theory ($Z > 2.3$; $p < 0.05$, corrected).

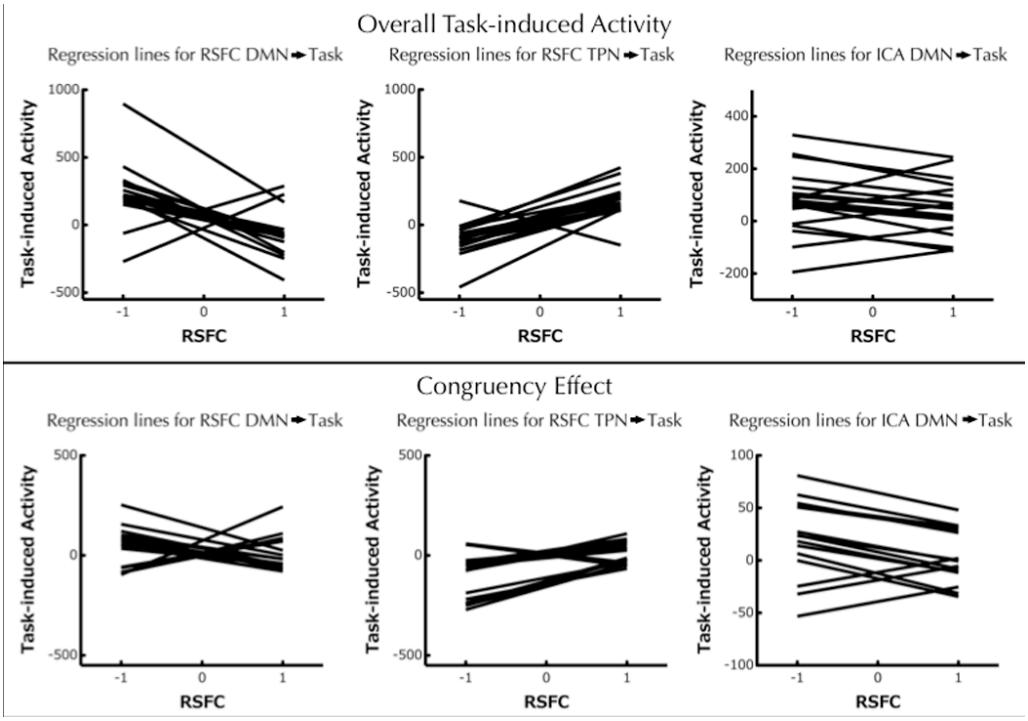

Figure 4. Regression lines representing the relationship between RSFC for the default mode, task-positive or ICA-based default mode network, and task-induced activity

Each line represents the linear relationship between RSFC (X axis) with the default mode network map (left), task-positive network map (middle), or ICA-based default mode network (right) and task-induced activity (Y axis) for each of the yellow regions shown in Figures 3 and 5. Top: graphs showing the relationship between RSFC and overall task-induced activity (Congruent + Incongruent > Baseline); Bottom: graphs showing the relationship between RSFC and task-induced activity associated with the congruency effect (Incongruent > Congruent).

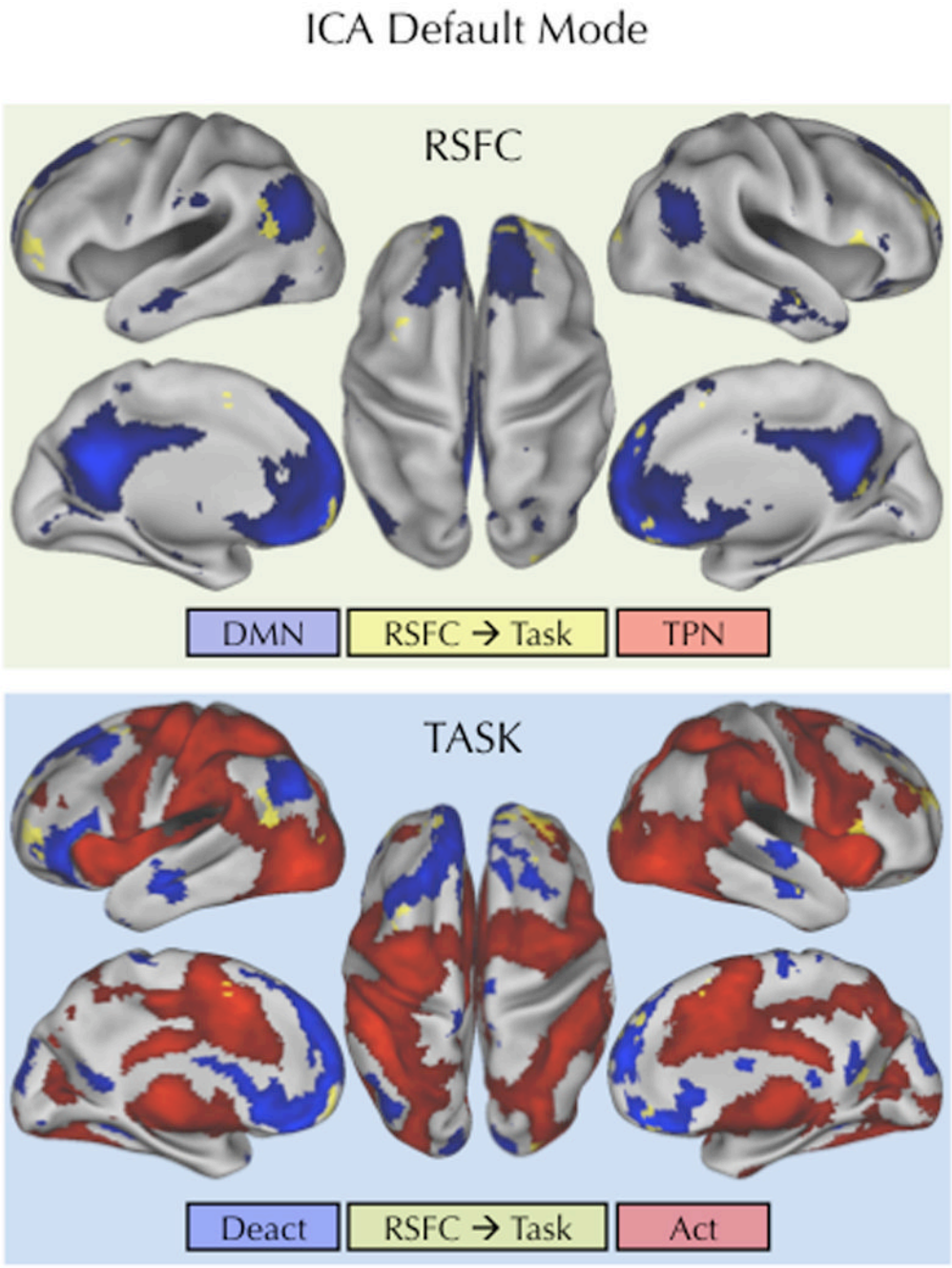

Figure 5. RSFC for the default mode ICA component significantly predicted overall task- induced activity

Regions (yellow) showing a significant relationship between RSFC for the ICA-based default mode component and overall task-induced activity (Congruent + Incongruent > Baseline) are overlaid on the default mode ICA component (blue). The bottom figure shows the same significant regions overlaid on overall task-induced activations (red) and deactivations (blue). Statistical maps were corrected for multiple comparisons using Gaussian random field theory ($Z > 2.3$; $p < 0.05$, corrected).

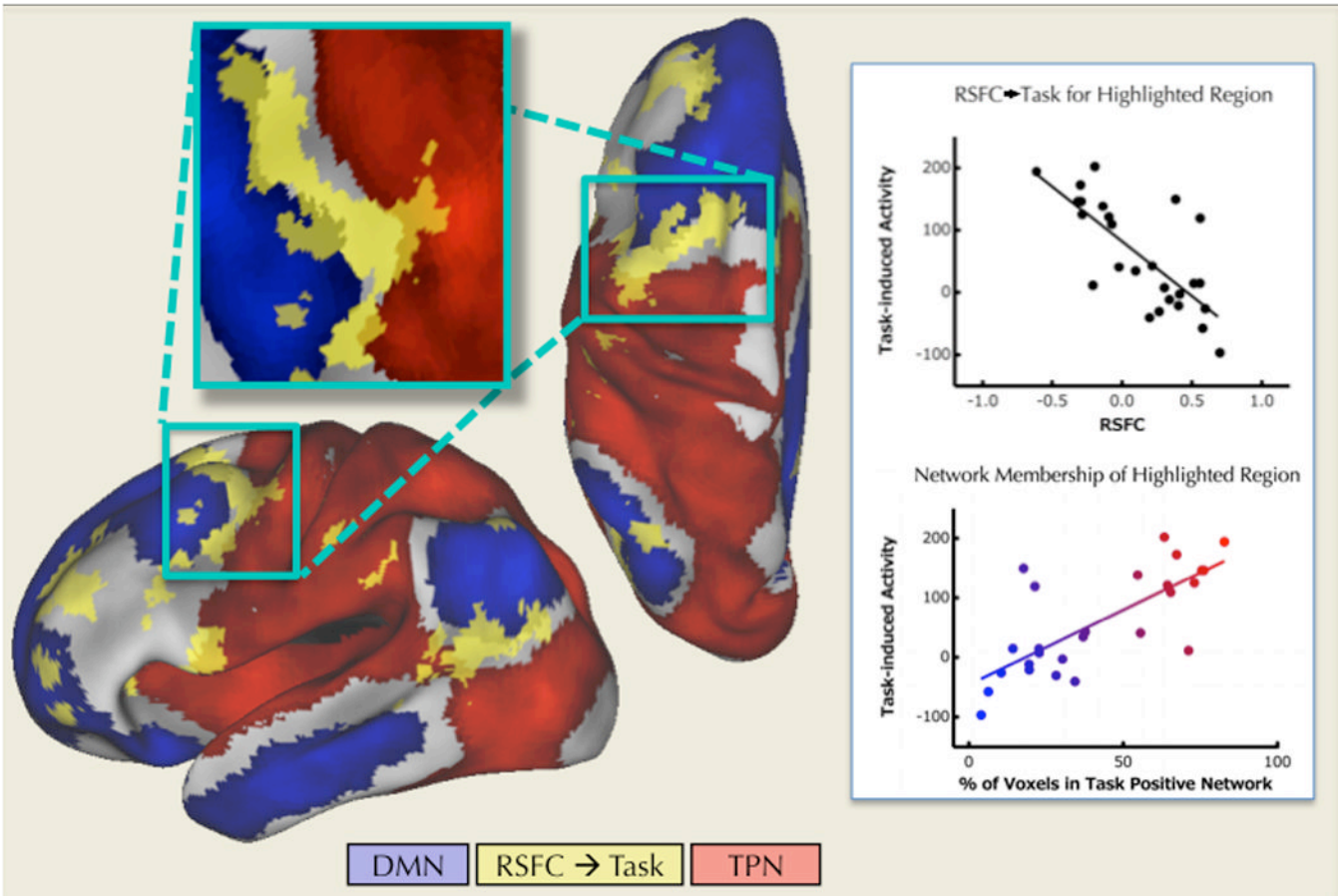

Figure 6. Network-membership predicted overall task-induced activity in *transition zones* between the default mode and task-positive resting-state networks

Regions (yellow) showing a significant relationship between RSFC with the default mode network map and overall task-induced activity (Congruent + Incongruent > Baseline) were often located within transition zones between the default mode (blue) and task-positive (red) resting state networks. The top graph illustrates the relationship between RSFC (X axis) and overall task-induced activity (Y axis) across participants (black dots) for the dorsolateral prefrontal region highlighted on the surface map. For this same region, the bottom graph on the right illustrates the relationship across participants between the relative percentage of voxels that belonged to the task-positive network (relative % = [% TPN / (% TPN + % DMN)]) (X axis) and overall task-induced activity (Y axis). Statistical maps were corrected for multiple comparisons using Gaussian random field theory ($Z > 2.3$; $p < 0.05$, corrected).

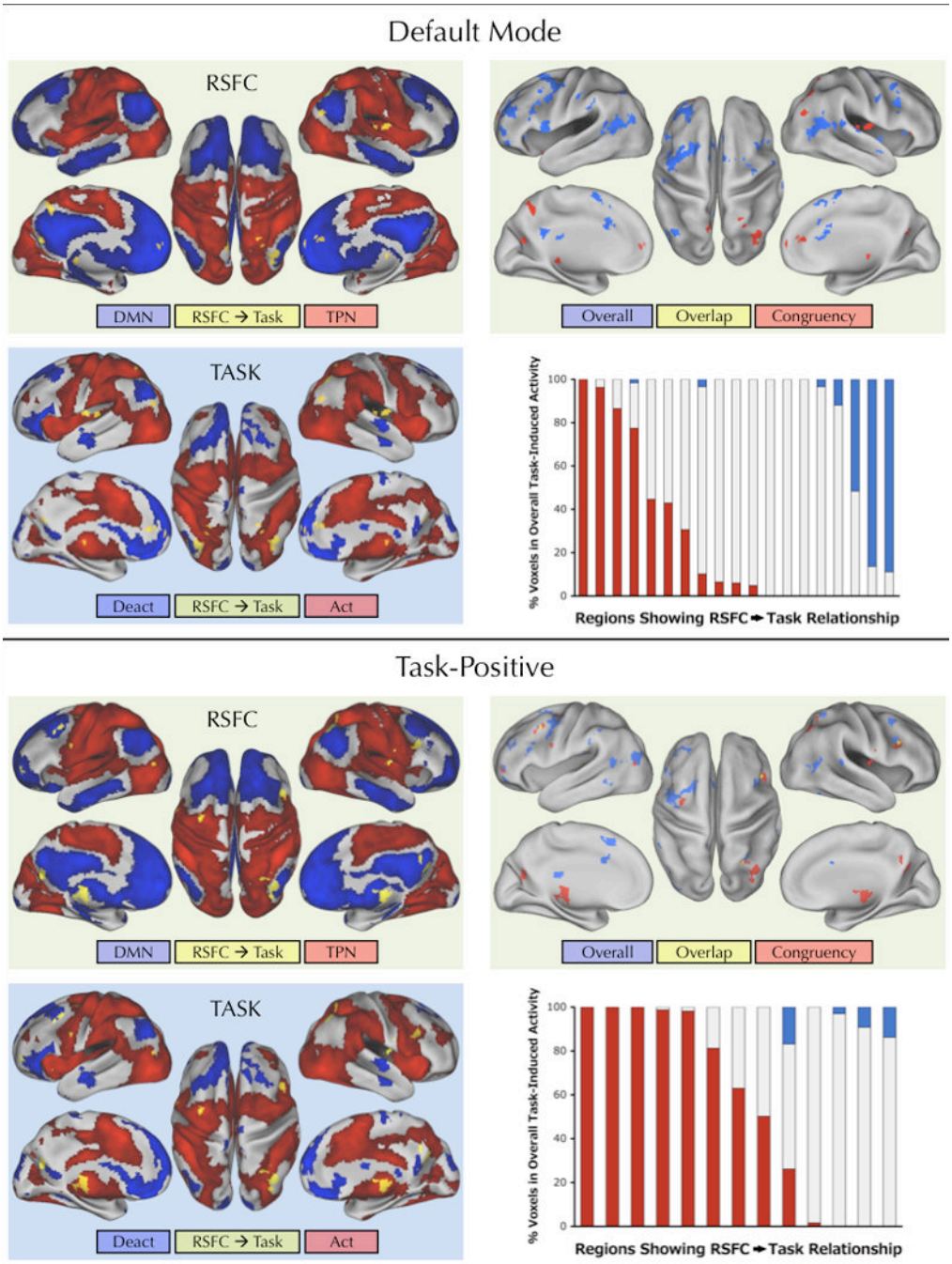

Figure 7. RSFC significantly predicted BOLD activity associated with the congruency effect

The top half of the figure illustrates regions (yellow) showing a significant relationship between RSFC with the default mode network map and task-induced activity associated with the congruency effect (Incongruent > Congruent). On the "RSFC" surface maps on the left, regions showing a significant RSFC/task-induced activity relationship (yellow) are overlaid on the default mode (blue) and task-positive (red) resting-state networks. The "TASK" surface maps show the same yellow regions overlaid on overall task-induced activations (red) or deactivations (blue) (Congruent + Incongruent > Baseline). The surface maps on the right illustrate regions showing a significant relationship between RSFC based on the default mode network map seed and overall task-induced activity (blue) in comparison to regions showing

a significant relationship between RSFC with the default mode network map and task activity induced by the congruency effect (red). Overlapping regions are shown in yellow; only 4% of the voxels obtained for the congruency effect analysis (Incongruent > Congruent) were also found in the overall task-induced analysis (Congruent + Incongruent > Baseline). For each region that showed a significant relationship between RSFC with the default mode network map and task-induced activity related to the congruency effect (yellow regions in surface maps on the left), the bar graph indicates the relative percentage of voxels in that region that overlapped with overall task-induced activation (red) or deactivation (blue) (relative % = [% activation / (% activation + % deactivation)]). The bottom half of the figure identically illustrates the results for the analyses using RSFC with the task-positive network map. For the task-positive network map analyses only 7% of the voxels obtained for the congruency effect (Incongruent > Congruent) were also found in the overall task-induced analysis (Congruent + Incongruent > Baseline). Statistical maps were corrected for multiple comparisons using Gaussian random field theory ($Z > 2.3$; $p < 0.05$, corrected).